IEEE Access
Multidisciplinary | Rapid Review | Open Access Journal

Received June 8, 2022, accepted June 15, 2022, date of publication June 20, 2022, date of current version June 23, 2022.

Digital Object Identifier 10.1109/ACCESS.2022.3184295

Design of Bandpass Multiplexer-Integrated Power Dividers

CHI-FENG CHEN, (Member, IEEE), HSIN-YA TSENG, YI-HUA HE, AND WEN-JIE LE
Department of Electrical Engineering, Tunghai University, Taichung 40704, Taiwan

Corresponding author: Chi-Feng Chen (cfchen@thu.edu.tw)

This work was supported by the Ministry of Science and Technology, Taiwan, under Grant MOST 109-2221-E-029-023 and Grant MOST 110-2221-E-029-013.

ABSTRACT This study proposed a novel methodology for designing bandpass multiplexer-integrated power dividers (PDs) that provide frequency division, frequency selection, and power division. New coupling schemes for the multiplexer-integrated PDs were presented to ensure multifunctionality and compactness. Miniaturization was achieved through the common resonator technique. Dual-mode stub-loaded resonators serving as common resonators for various channel passbands were used in the multiplexer-integrated PD to reduce the required number of resonators and thereby considerably reduce the size. Each channel passband can be individually designed using the distributed coupling technique to decrease complexity. For validation, a third-order bandpass triplexer-integrated PD and third-order bandpass quad-channel diplexer-integrated PD were designed and fabricated using microstrip technology. Measurements of the devices were consistent with simulated results. The proposed circuits are compact, multifunctional, highly integrate, high performing, simple, and easy to fabricate; thus, they are suitable for the practical applications, such as multi-standard operation antenna array modules.

INDEX TERMS Bandpass filter (BPF), diplexer, multifunction, power divider (PD), triplexer.

I. INTRODUCTION

Compact, high-performance, multifunctional microwave circuits have attracted widespread attention and are increasingly being applied in multiband wireless and mobile communication systems. Multifunctional circuits can facilitate system integration and reduce system size and cost. Numerous studies have reported multifunctional circuit design elements such as the filtering power divider (PD), duplexing filtering PD, balun filter, and filtering antenna; various design methodologies have also been proposed.

Filtering PD designs that integrate a bandpass filter (BPF) and PD into a circuit and offer frequency selection and power division have been proposed. The filtering PDs in [1]–[6] were designed using the coupled-resonator technique. Because these filtering PDs were constructed with miniaturized resonators, the overall circuit area was small. To further reduce circuit size, multimodal, resonator-based filtering PDs have also been investigated [7]–[20]. In [7]–[9], dual- and tri-mode resonators were used to produce a filtering PD. Strong isolation performance was achieved by including an isolation resistor between the two resonators. In [10], a single open-type dual-mode resonator and a resistor were integrated into a filtering PD design. Three open-ended stubs were introduced to increase the frequency selectivity and enhance the stopband response of the PD. In [11]–[14], multiway filtering PDs were explored for multichannel applications. Numerous examples of tunable filtering PDs [11], [15], [21]–[25] with wideband operations [7], [12], [15], [26]–[28] have been reported. In [11] and [15], varactor-tuned multimode stub-loaded resonators were used to design reconfigurable filtering PDs with tunable center frequencies, bandwidth, and power division. In [21] and [22], tunable filtering PDs produced using a varactor-loaded coupled-resonator topology were proposed. In [23], filtering PDs based on quasi-bandpass sections were reported; these PDs feature frequency-controllable single-band and multiband operations. In [24], Wilkinson-type PDs with reconfigurable quasi-elliptic-type filtering characteristics were reported; the center frequency, bandwidth, stopband bandwidth, and out-of-band attenuation of these PDs are reconfigurable through dynamic transmission-zero allocation. In [25], a reconfigurable filtering PD design method based on a flexible tunable coupling topology that ensured compactness and a

The associate editor coordinating the review of this manuscript and approving it for publication was Photos Vryonides.

wide frequency tunning range was proposed. In [26]–[28], wideband filtering PDs based on a parallel-coupled line structure were proposed; these PDs also achieved a satisfactory stopband response. In addition, [11], [13], [16]–[20], and [29]–[36] developed filtering PDs for dual-band applications. By assigning the resonance frequencies of one or more multimode resonators, filtering PDs with dual-band behavior have been created [11], [13], [16]–[20]. In [29], [30], and [34], dual-resonance resonators were applied to design PDs with dual-band filtering responses. In [31], T-junction structures and quarter-wavelength stepped impedance resonators were employed in a Wilkinson PD design, which achieved dual-band power allocation and a bandpass response. The filtering PD in [32] was designed to achieve a dual-band filtering response with arbitrary power division, an arbitrary frequency ratio, arbitrary real terminated impedances, and independently controllable bandwidth by replacing the conventional quarter-wavelength transmission line with a dual-band filtering structure. The filtering PD in [33] was constructed using two open-stub resonators loaded on both side lines of a three-line coupled structure to ensure a dual-wideband bandpass response. In [35] and [36], dual-band filtering PDs based on single-layer substrate-integrated waveguide cavities were proposed.

To improve the functions of single circuits, various diplexer-integrated filtering PD (or duplexing filtering PD) designs that can provide frequency division, frequency selection, and power division have been developed [37]–[42]. The designs in [37]–[40] and [42] were for two-channel applications, and the design in [41] was for three-channel applications. Each of these circuits was designed to have a second-order bandpass response, resulting in poor selectivity. However, with the rapid development of modern wireless communications, the demand for multifunctional multiplexers with several operating channels and strong performance has increased. The conventional method for achieving frequency division, frequency selection, and power division typically requires numerous circuits, including a matching network, BPFs, and PDs (Fig. 1). These circuits increase the size and cost of a system. This problem can be resolved by integrating BPFs, PDs, and multiplexers into a single circuit, namely a bandpass multiplexer-integrated PD (Fig. 1). This study proposed a novel methodology for the design of a bandpass multiplexer-integrated PD. To the best of the authors' knowledge, no bandpass multiplexer-integrated PD operating on more than three channel bands has been reported in the literature. For proof-of-concept purposes, a bandpass triplexer-integrated PD and a bandpass quad-channel diplexer-integrated PD were designed and implemented in microstrip technology. The experimental results indicate that the proposed structures have excellent filtering performance and port-to-port isolation. The proposed structures also have a small footprint and thus can be used for applications requiring miniaturization.

The remaining sections of this paper are organized as follows: Sections 2 and 3 detail the design methods, production procedures, and novel circuit topologies for the proposed novel bandpass triplexer-integrated PD and bandpass quad-channel diplexer-integrated PD, respectively. Design formulas for the proposed topologies are also provided. The results of two-port vector network analyzer measurements are also presented and compared with full-wave electromagnetic (EM) simulation results. In Section 4, the performance of the proposed circuits is compared with that of the state of the art, and the main contributions of the proposed bandpass multiplexer-integrated PDs are highlighted. Finally, Section 5 presents the conclusion.

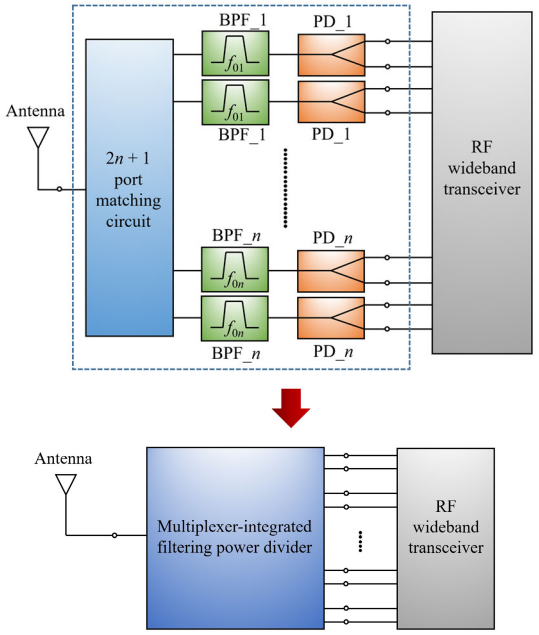

FIGURE 1. Simplified architecture of bandpass multiplexer-integrated PD.

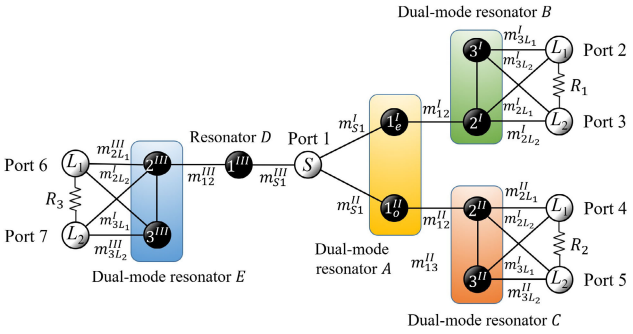

FIGURE 2. Coupling scheme of proposed bandpass triplexer-integrated PD. (third-order bandpass response).

II. DESIGN OF BANDPASS TRIPLEXER-INTEGRATED PD

Fig. 2 presents the coupling scheme of the proposed triplexer-integrated PD with a third-order bandpass response. The circuit is a seven-port network. The multifunctional triplexer comprises only five resonators (resonators A, B, C, D, and E) and three isolation resistors (R_1, R_2, and R_3), where S and L represent the input and output ports, respectively. To miniaturize the circuit, the first even-mode resonance

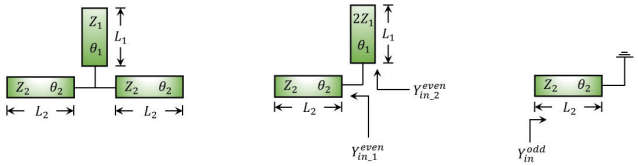

FIGURE 3. (a) Circuit model of dual-mode stub-loaded resonator. (b) Even-mode equivalent circuit. (c) Odd-mode equivalent circuit.

TABLE 1. Specification of bandpass triplexer-integrated PD.

Channel	I	II	III
Center frequency (GHz)	1.31	1.845	2.2
Bandwidth (MHz)	80	90	50
Filter order	3	3	3
Power division ratio	1:1	1:1	1:1

frequency of dual-mode resonator A (node 1_e^I) and the first even-mode and odd-mode resonance frequencies of dual-mode resonator B (nodes 2^I and 3^I) were used to form the operating passband of channel I; the first odd-mode resonance frequency of dual-mode resonator A (node 1_o^{II}) and the first even-mode and odd-mode resonance frequencies of dual-mode resonator C (nodes 2^{II} and 3^{II}) were used to form the operating passband of channel II. Finally, the fundamental resonance frequency of resonator D (node 1^{III}) and the first even-mode and odd-mode resonance frequencies of dual-mode resonator E (nodes 2^{III} and 3^{III}) were used to form the operating passband of channel III. A third-order bandpass response can thus be achieved for each channel passband. In addition, because an additional cross-coupling path exists in the coupling scheme, a transmission zero above the passband was generated for each channel [43]. If the output coupling structure is designed to be symmetrical, equal-power division with the in-phase property can be achieved for each channel. Three resistors, namely R_1, R_2, and R_3, loaded between the outputs enhance the impedance matching of and isolation between the output ports. The isolation resistors do not influence the power splitting or filtering performance [10]; thus, the resistances of the isolation resistors can be determined after all other design decisions are made.

The dual-mode stub-loaded resonator presented in Fig. 3(a) was employed in the design of the bandpass triplexer-integrated PD; Z_i, θ_i, and L_i ($i = 1, 2$) represent the characteristic impedance, electric length, and physical length of the transmission line, respectively. Because of the symmetric circuit structure of the dual-mode stub-loaded resonator, the resonance conditions can be analyzed with the even- and odd-mode equivalent circuits in Fig. 3(b) and (c), respectively. By setting the imaginary parts of Y_{in}^{even} ($Y_{in}^{even} = Y_{in\_1}^{even} + Y_{in\_2}^{even}$) and Y_{in}^{odd} equal to zero, the even- and odd-mode resonance conditions of the resonator can be expressed as follows:

$$\frac{1}{Z_2}\tan\theta_2 + \frac{1}{2Z_1}\tan\theta_1 = 0 \tag{1}$$

$$\cot\theta_2 = 0 \tag{2}$$

With these resonance conditions, the even- and odd-mode resonance frequencies of the dual-mode stub-loaded resonator f_e and f_o can be calculated by assuming $Z_2 = 2Z_1$ as follows [8]–[10]:

$$f_e = \frac{c}{2\left(L_1 + L_2\right)\sqrt{\epsilon_e}} \tag{3}$$

$$f_o = \frac{c}{4L_2\sqrt{\epsilon_e}} \tag{4}$$

where c is the speed of an electromagnetic wave in a vacuum and ϵ_e is the effective dielectric constant of the substrate. Equation (4) indicates that odd-mode resonant frequency f_o depends only on L_2. Therefore, in the resonator design, f_o can be determined by adjusting L_2. Subsequently, even-mode resonant frequency f_e can be determined by adjusting L_1 accordingly.

To experimentally verify the proposed design, a bandpass triplexer-integrated PD was produced using microstrip technology. The Rogers RO4003C laminate with a dielectric constant of 3.55, thickness of 0.508 mm, and loss tangent of 0.0027 was used for design and fabrication. The design specifications of the bandpass triplexer-integrated PD are listed in Table 1. For each given specification, the coupling matrix for channel N can be synthesized and expressed as follows:

$$[m]^N = \begin{bmatrix} m_{SS} & m_{S1} & m_{S2} & m_{S3} & m_{SL_1} & m_{SL_2} \\ m_{1S} & m_{11} & m_{12} & m_{13} & m_{1L_1} & m_{1L_2} \\ m_{2S} & m_{21} & m_{22} & m_{23} & m_{2L_1} & m_{2L_2} \\ m_{3S} & m_{31} & m_{32} & m_{33} & m_{3L_1} & m_{3L_2} \\ m_{L_1S} & m_{L_1}1 & m_{L_1}2 & m_{L_1}3 & m_{L_1L_1} & m_{L_1L_2} \\ m_{L_2S} & m_{L_2}1 & m_{L_2}2 & m_{L_2}3 & m_{L_2L_1} & m_{L_2L_2} \end{bmatrix}$$

$$= \begin{bmatrix} 0 & 1.083 & 0 & 0 & 0 & 0 \\ 1.083 & 0.121 & 1.062 & 0 & 0 & 0 \\ 0 & 1.062 & 0.43 & 0.776 & 0.358 & 0.358 \\ 0 & 0 & 0.776 & -0.785 & 0.677 & 0.677 \\ 0 & 0 & 0.358 & 0.677 & 0 & 0 \\ 0 & 0 & 0.358 & 0.677 & 0 & 0 \end{bmatrix}$$

$$N = \text{I, II, III} \tag{5}$$

To achieve an equal-split filtering response, the normalized coupling coefficient in (5) should satisfied the conditions of $m_{2L_1} = m_{2L_2} = m_{2L}/\sqrt{2}$ and $m_{3L_1} = m_{3L_2} = m_{3L}/\sqrt{2}$, while m_{2L} and m_{3L} are the output couplings for a third-order BPF with a single output. Therefore, the external quality factors for two output ports are equal to each other, which are twice values of the output external quality factor for a third-order BPF with a single output. Fig. 4 shows the ideal response of the bandpass triplexer-integrated PD. Fig. 5 presents the layout of the proposed triplexer-integrated PD. Only five resonators are required for this design. Resonator D was a half-wavelength resonator; resonators A, B, C, and E were the dual-mode stub-loaded resonators. The distributed coupling technique was used to integrate the three-channel filtering PDs without an extra matching circuit,

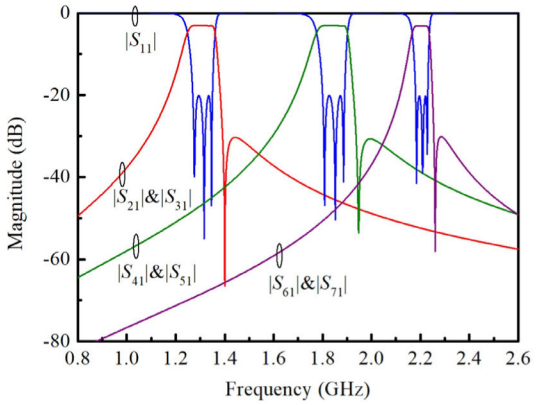

FIGURE 4. Ideal response of proposed bandpass triplexer-integrated PD.

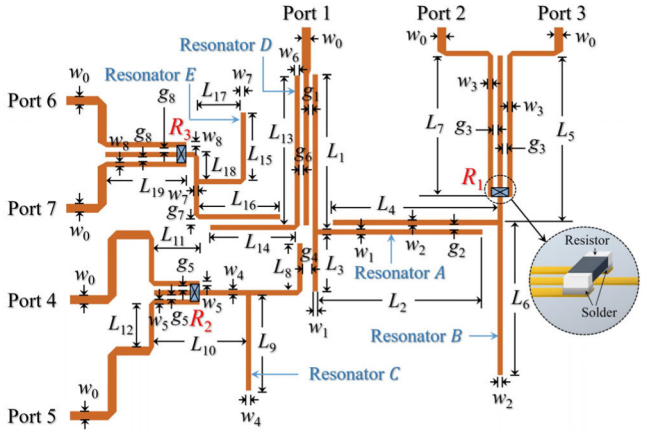

FIGURE 5. Microstrip structure of proposed bandpass triplexer-integrated PD.

TABLE 2. Dimensions of bandpass triplexer-integrated PD. (unit: mm).

L_1	L_2	L_3	L_4	L_5	L_6	L_7	L_8
33	35.1	12.1	35.1	35	31.9	30	10
L_9	L_{10}	L_{11}	L_{12}	L_{13}	L_{14}	L_{15}	L_{16}
20.3	19.6	9.7	9	31.8	18	14.2	17.3
L_{17}	L_{18}	L_{19}	w_0	w_1	w_2	w_3	w_4
9	4.8	17	1.8	1	1	1	1
w_5	w_6	w_7	w_8	g_1	g_2	g_3	g_4
1	1	1	1	0.1	0.98	0.56	1.45
g_5	g_6	g_7	g_8				
0.45	0.11	0.73	0.58				

thereby reducing circuit size. The loading effects between channel passbands were weak because of the use of this distributed coupling structure [42]. As a result, each of the three-channel passbands can be designed individually.

The desired resonance frequencies of each resonator can be derived as follows [44]:

$$f_i^N = f_0^N \left(1 - \frac{m_{ii}^N}{2}\right) \quad i = 1, 2, 3 \tag{6}$$

where f_0^N and m_{ii}^N denote the center frequency of the passband and normalized coupling coefficient, respectively, for channel N. On the basis of the specifications, the desired resonance frequencies of the resonators were calculated: $f_1^I = 1.3$ GHz, $f_2^I = 1.29$ GHz, $f_3^I = 1.34$ GHz, $f_1^{II} = 1.84$ GHz,

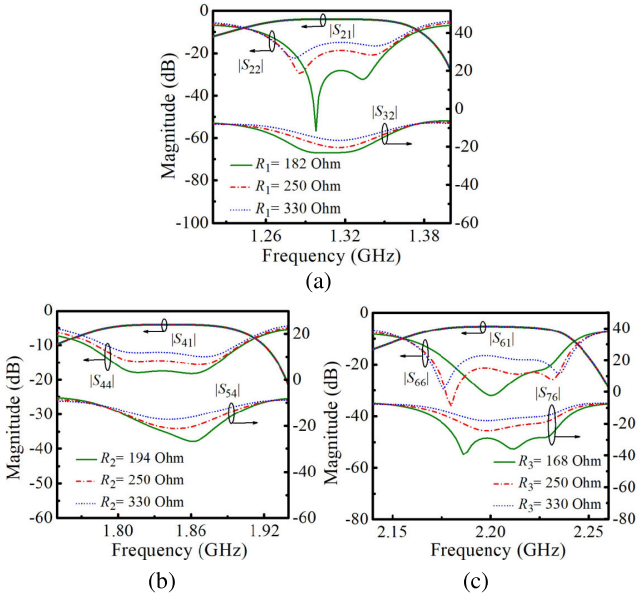

FIGURE 6. Simulated frequency responses with variations in resistances for (a) channel *I*, (b) channel *II*, and (c) channel *III*.

$f_2^{II} = 1.82$ GHz, $f_3^{II} = 1.88$ GHz, $f_1^{III} = 2.2$ GHz, $f_2^{III} = 2.19$ GHz, and $f_3^{III} = 2.23$ GHz. The geometric parameters of the dual-mode stub-loaded resonators are determined using (3) and (4).

Coupling coefficient M_{ij} is given by the following:

$$M_{ij} = m_{ij} \cdot FBW \tag{7}$$

where m_{ij} and FBW (the ratio of the passband bandwidth to the center frequency of the passband) are the normalized coupling coefficient and fractional bandwidth, respectively. The coupling coefficient depends on the distance between the adjacent resonators and can be extracted using a full-wave simulator through the following formula [44]:

$$M_{ij} = \frac{1}{2}\left(\frac{f_{02}}{f_{01}} + \frac{f_{01}}{f_{02}}\right)\sqrt{\left(\frac{f_{p2}^2 - f_{p1}^2}{f_{p2}^2 + f_{p1}^2}\right) - \left(\frac{f_{02}^2 - f_{01}^2}{f_{02}^2 + f_{01}^2}\right)} \tag{8}$$

where f_{0i} for $i = 1, 2$ represents the self-resonance frequencies of two adjacent resonators and f_{pi} for $i = 1, 2$ denotes the two split frequencies for two resonators coupled with each other.

Input and output external quality factors Q_{ei} and Q_{eo}, respectively, can be derived as follows [44]:

$$Q_{ei} = \frac{1}{FBW \cdot m_{S1}^2} \tag{9}$$

$$Q_{eo,n} = \frac{1}{2}\left(\frac{1}{FBW \cdot m_{2L_n}^2} + \frac{1}{FBW \cdot m_{3L_n}^2}\right) \quad n = 2, 3 \tag{10}$$

To achieve a third-order filtering response with equal power splitting at two output ports, the required external quality factors were as follows: $Q_{ei}^I = 13.96$, $Q_{eo,2}^I = Q_{eo,3}^I = 40.89$, $Q_{ei}^{II} = 17.47$, $Q_{eo,2}^{II} = Q_{eo,3}^{II} = 49.13$,

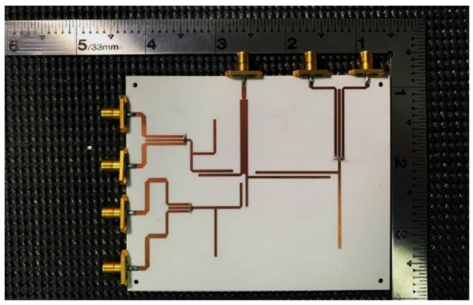

FIGURE 7. Photograph of bandpass triplexer-integrated PD.

$Q_{ei}^{III} = 37.6$, and $Q_{eo,2}^{III} = Q_{eo,3}^{III} = 105.72$. To satisfy these desired external quality factor requirements, the geometric parameters, namely line width, line length, and spacing of the I/O coupled lines were adjusted. External quality factors can be extracted using a full-wave simulator through the following formula [44]:

$$Q_e = \omega_0 \tau_d (f_0) / 4 \tag{11}$$

where $\tau_d (f_0)$ is the group delay of S_{11} at resonance frequency f_0.

The initial geometric parameters for the bandpass triplexer-integrated PD were determined when the extracted values of coupling coefficients and external quality factors corresponded to the theoretical values. By using to this design procedure, the initial geometric parameters for the bandpass triplexer-integrated PD can be obtained. When an equal-split filtering response was achieved at each channel, the isolation between the output ports and the impedance matching of the output ports for each channel was enhanced by changing the resistances of isolation resistors R_1, R_2, and R_3. Fig. 6(a)–(c) displays the simulated frequency responses with various resistances for R_1, R_2, and R_3, respectively. Output return losses $|S_{22}|$, $|S_{44}|$, and $|S_{66}|$ and port-to-port isolations $|S_{32}|$, $|S_{54}|$, and $|S_{76}|$ change with the resistances of R_1, R_2, and R_3, respectively, with a negligible effect on the equal-power splitting and filtering performances. The initial values of the resistances can be obtained using the matching condition of the output for each channel. The optimized resistances of the three resistors were $R_1 = 182\ \Omega$, $R_2 = 194\ \Omega$, and $R_3 = 168\ \Omega$ to achieve high isolation and impedance matching. A fine-tuning procedure can be performed to optimize performance if required; the produced multifunctional PDs were fine-tuned in this study. The proposed bandpass triplexer-integrated PD has been fabricated using a conventional printed circuit board (PCB) process. A photograph of the fabricated bandpass triplexer-integrated PD is displayed in Fig. 7, and its physical dimensions are presented in Table 2. The circuit size was $0.63\ \lambda_g \times 0.48\ \lambda_g$ (93.9 mm × 72.1 mm), where λ_g is the guided wavelength at 1.31 GHz.

Simulations were performed with a full-wave EM simulator (Keysight Advanced Design System, ADS), and measurements were performed with the Agilent N5230A network analyzer. And a short-open-load-thru method was used for calibration. The S-parameter measurements have been performed from 0.8 up to 2.6 GHz. Since the proposed bandpass triplexer-integrated PD is a seven-port device, 50-Ω loads need to be used generally. During measurements, ports i and j (i, j = 1 to 7) of the device are connected to the 2-port network analyzer for obtaining input and output matching, transmission, and phase response between ports i and j, while the other ports should be loaded at 50-Ω loads. Figs. 8, 9, and 10 present plots of the EM simulated and measured frequency responses of the proposed bandpass triplexer-integrated PD. A filtering response with equal-power division was accomplished in each channel. The experimental results indicate that the in-band return losses ($-20 \log |S_{11}|$) were higher than 15 dB and that the in-band insertion losses ($-20 \log |S_{21}|$, $-20 \log |S_{41}|$, and $-20 \log |S_{61}|$) at channel passbands *I*, *II*, and *III*, respectively, including the 3-dB equal-power division loss, were approximately (3 + 1.0), (3 + 0.9), and (3 + 2.9) dB, respectively. The isolations between the output ports ($-20 \log |S_{32}|$, $-20 \log$

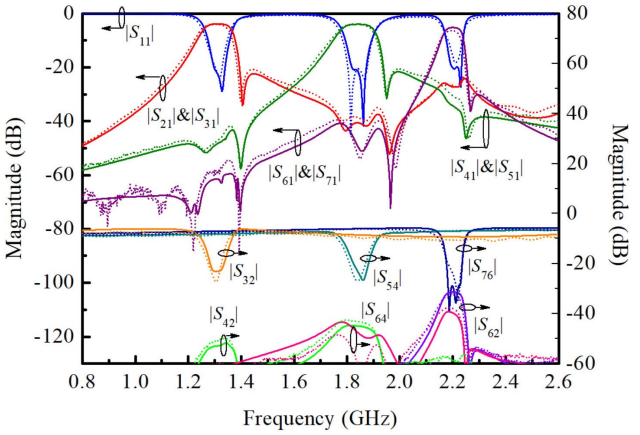

FIGURE 8. Simulated and measured frequency responses of proposed bandpass triplexer-integrated PD. (simulation: solid curves; measurement: dotted curves).

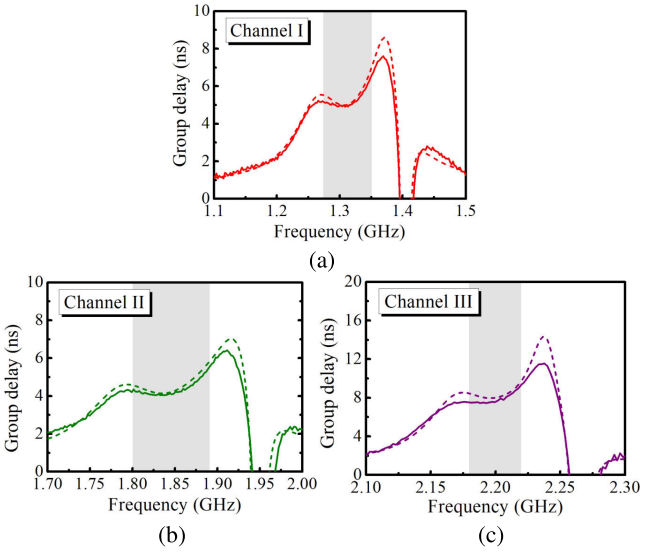

FIGURE 9. Simulated (dashed lines) and measured (solid lines) group delay of proposed bandpass triplexer-integrated PD for (a) channel I, (b) channel II, and (c) channel III.

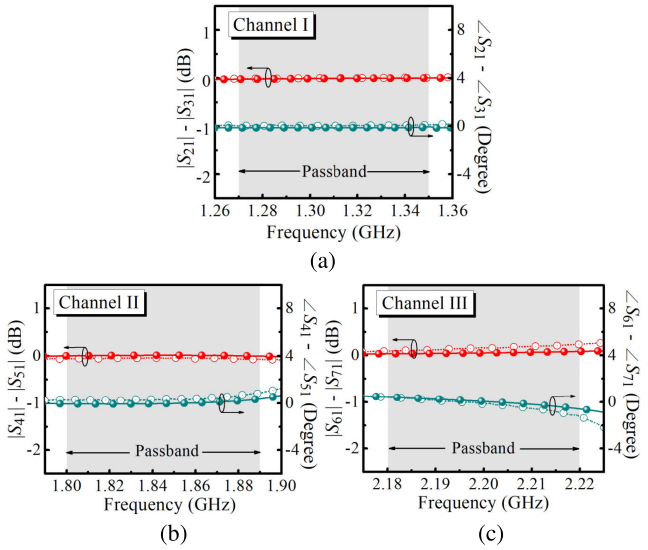

FIGURE 10. Magnitude and phase imbalances for (a) channel I, (b) channel II, and (c) channel III. (simulation: solid curves; measurement: dotted curves).

$|S_{54}|$, and -20 log $|S_{76}|$) were greater than 25 dB over the entirety of the channel passbands. The port isolations between channels (-20 log $|S_{42}|$, -20 log $|S_{62}|$, and -20 log $|S_{64}|$) were greater than 31 dB. A transmission zero generated above the passband was observed, which greatly increases the skirt selectivity for each channel. The measured in-band group delay for the first, second, and third channel passbands are 4.92–6.44 ns, 4.04–4.99 ns, and 7.44–9.31 ns, respectively. In addition, the amplitude and phase imbalances within the passbands were <0.25 dB and <2°, respectively. As a result, the measured and simulated results were consistent, which validates the proposed design method.

III. DESIGN OF BANDPASS QUAD-CHANNEL DIPLEXER-INTEGRATED PD

Fig. 11 presents the coupling scheme of the proposed third-order bandpass quad-channel diplexer-integrated PD, which mainly comprises eight resonators (resonators $1^{I,III}$, 2^{I}, 2^{III}, $3^{I,III}$, $1^{II,IV}$, 2^{II}, 2^{IV}, and $3^{II,IV}$) and two isolation resistors (R_1 and R_2), where S and L denote the input and output ports, respectively. The circuit is a five-port network. In this design, the fundamental resonance frequency of the resonator 2^{I} (node 2^{I} @ f_{01}) and first even-mode resonance frequencies of dual-mode resonators $1^{I,III}$ and $3^{I,III}$ (nodes 1^{I}_{e} and 3^{I}_{e} @ f_{01}) were used to form the operating passband of channel I; the fundamental resonance frequency of resonator 2^{II} (node 2^{II} @ f_{02}) and first even-mode resonance frequencies of dual-mode resonators $1^{II,IV}$ and $3^{II,IV}$ (nodes 1^{II}_{e} and 3^{II}_{e} @ f_{02}) were used to form the operating passband of channel II; the fundamental resonance frequency of the resonator 2^{III} (node 2^{III} @ f_{03}) and first odd-mode resonance frequencies of resonators $1^{I,III}$ and $3^{I,III}$ (nodes 1^{III}_{o} and 3^{III}_{o} @ f_{03}) were used to form the operating passband of channel III; the fundamental resonance frequency of the resonator 2^{IV} (node 2^{IV} @ f_{04})

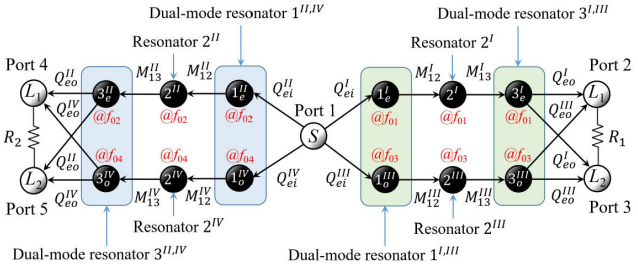

FIGURE 11. Coupling scheme of proposed bandpass quad-channel diplexer-integrated PD. (third-order bandpass response).

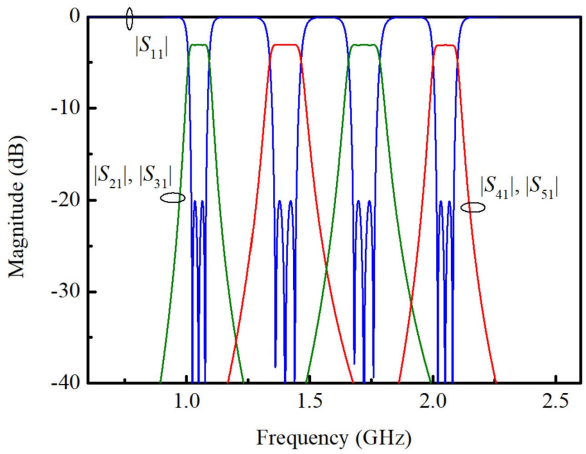

FIGURE 12. Ideal response of proposed bandpass quad-channel diplexer-integrated PD.

and first odd-mode resonance frequencies of resonators $1^{II,IV}$ and $3^{II,IV}$ (nodes 1^{IV}_{o} and 3^{IV}_{o} @f_{04}) were used to form the operating passband of channel IV. A third-order bandpass response can thus be achieved for each channel passband. The filter order and selectivity can be increased by adding resonators to each coupling path. Because the proposed circuit has an independent signal coupling path for each operating frequency band, each of the channel passbands can be created individually. The topology of the symmetrical output feeding structure enables an equal-power division function with the in-phase property for each channel. In addition, two resistors, namely R_1 and R_2, were loaded between the outputs to improve the isolation between output ports and the impedance matching of the output ports for each channel.

To verify the proposed design methodology, the third-order bandpass quad-channel diplexer-integrated PD was implemented using microstrip technology. Rogers RO4003C with a dielectric constant of 3.55, thickness of 0.508 mm, and loss tangent of 0.0027 was used as the dielectric substrate. The design specifications of the bandpass quad-channel diplexer-integrated PD are listed in Table 3. Fig. 12 shows the ideal response of the bandpass quad-channel diplexer-integrated PD. The required coupling coefficient between adjacent resonators and the I/O external quality factor can be calculated using the following formulas [44]:

$$M_{ij}^{N} = \frac{FBW^{N}}{\sqrt{g_i g_{i+1}}} \tag{12}$$

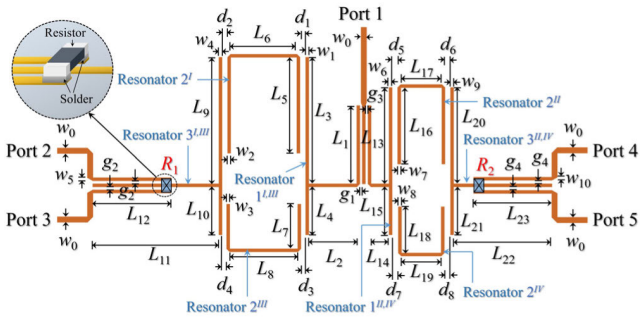

FIGURE 13. Microstrip structure of proposed bandpass quad-channel diplexer-integrated PD.

TABLE 3. Specification of quad-channel diplexer-integrated PD.

Channel	I	II	III	IV
Center frequency (GHz)	1.05	1.4	1.72	2.05
Bandwidth (MHz)	60	90	90	70
Filter order	3	3	3	3
Power division ratio	1:1	1:1	1:1	1:1

$$Q_{ei}^{N} = \frac{g_0 g_1}{FBW^{N}} \tag{13}$$

$$Q_{eo}^{N} = 2 \cdot \frac{g_0 g_1}{FBW^{N}} \tag{14}$$

where g_i is the lumped circuit element values of the low-pass prototype filter and superscript N is the channel number ($N = I$, II, III, or IV). Output external quality factor Q_{eo}^{N} is two times input external quality factor Q_{ei}^{N} because the energy is equally split into two outports for each channel. The layout of the third-order bandpass quad-channel diplexer-integrated PD is displayed in Fig. 13. Resonators 2^{I}, 2^{II}, 2^{III}, and 2^{IV} were created with the U-shaped half-wavelength resonator, and resonators $1^{I,III}$, $3^{I,III}$, $1^{II,IV}$, and $3^{II,IV}$ were created with the dual-mode stub-loaded resonator in Fig. 3. The design was miniaturized because of the reduction in number of resonators to eight (in general, twelve resonators are required for a third-order quad-channel diplexer). The design does not require a matching network at the input because the distributed coupling technique was used. Moreover, the four channel passbands can be designed individually.

On the basis of the specifications, the desired coupling coefficients between adjacent resonators can be calculated using (12):$M_{12}^{I} = M_{23}^{I} = 0.059$, $M_{12}^{II} = M_{23}^{II} = 0.067$, $M_{12}^{III} = M_{23}^{III} = 0.054$, and $M_{12}^{IV} = M_{23}^{IV} = 0.035$. The coupling coefficients can be extracted using the full-wave simulator through (8). If the extracted value of the coupling coefficient is equal to the theoretical value, the distance between the adjacent resonators can be determined. The desired I/O external quality factors can be calculated using (13) and (14): $Q_{ei}^{I} = 14.9$, $Q_{eo}^{I} = 29.8$, $Q_{ei}^{II} = 13.1$, $Q_{eo}^{II} = 26.2$, $Q_{ei}^{III} = 16.4$, $Q_{eo}^{III} = 32.8$, $Q_{ei}^{IV} = 25$, and $Q_{eo}^{IV} = 50$. The external quality factor, which depends on line width, line length, and spacing of the I/O coupled lines, can be extracted using a full-wave simulator through (11). If the extracted external quality factors are equal to the theoretical values, the I/O coupling structure can be determined.

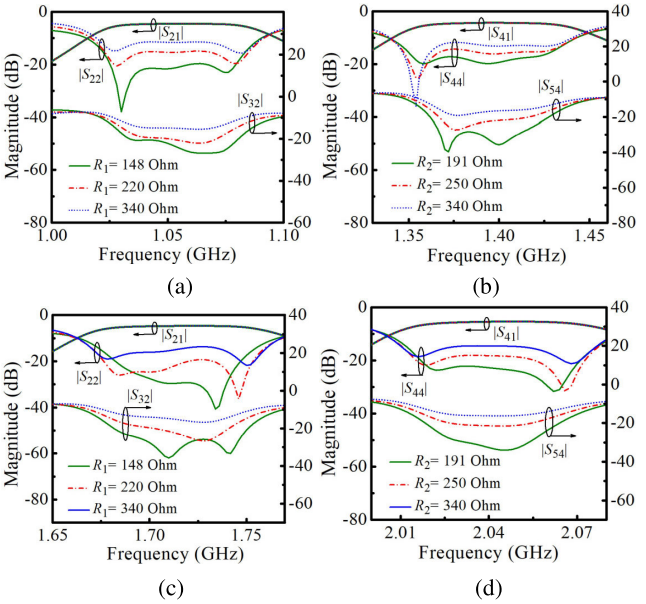

FIGURE 14. Simulated frequency responses with variation in resistances for (a) channel *I*, (b) channel *II*, (c) channel *III*, and (d) channel *IV*.

TABLE 4. Dimensions of bandpass quad-channel diplexer-integrated PD. (unit: mm).

L_1	L_2	L_3	L_4	L_5	L_6	L_7	L_8
26	16	42	16	31.85	22.04	14.75	22.66
L_9	L_{10}	L_{11}	L_{12}	L_{13}	L_{14}	L_{15}	L_{16}
42	16	41.96	26	32	6	16	25.4
L_{17}	L_{18}	L_{19}	L_{20}	L_{21}	L_{22}	L_{23}	w_0
13.69	15.3	13.25	32	16	32.7	26	1.8
w_1	w_2	w_3	w_4	w_5	w_6	w_7	w_8
1	1	1	1	1	1	1	1
w_9	w_{10}	d_1	d_2	d_3	d_4	d_5	d_6
1	1	1.18	1.18	0.87	0.87	1.18	1.18
d_7	d_8	g_1	g_2	g_3	g_4		
1.4	1.4	0.13	0.33	0.21	0.49		

After an equal-split filtering response was achieved at each channel, the isolation between the output ports and the impedance matching of output ports for each channel was improved. Resistors R_1 and R_2 were loaded between the output feeding lines (Fig. 13). Fig. 14 presents the simulated frequency responses for various values of R_1 and R_2. Output return losses $|S_{22}|$ and $|S_{44}|$ and port-to-port isolations $|S_{32}|$ and $|S_{54}|$ change with the resistances of resistors R_1 and R_2, respectively, with a negligible effect on the equal-power splitting and filtering performance. For channels *I* and *III*, both return loss ($|S_{22}|$) and isolation ($|S_{32}|$) increase if R_1 is changed from 340 to 148 Ω. Similarly, for channels *II* and *IV*, both return loss ($|S_{44}|$) and isolation ($|S_{54}|$) increase if R_2 is changed from 340 to 191 Ω. The initial values of the resistances can be obtained using the output matching condition. The optimized resistances for the two resistors were $R_1 = 148$ Ω and $R_2 = 191$ Ω. Finally, a fine-tuning procedure can be performed to optimize performance. A photograph of the fabricated bandpass quad-channel diplexer-integrated PD is displayed in Fig. 15, and its physical dimensions are listed

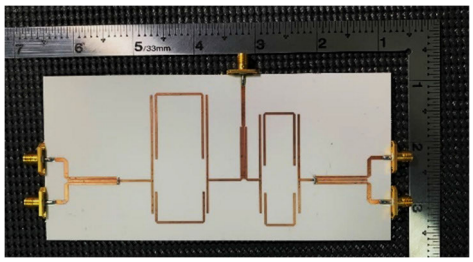

FIGURE 15. Photograph of fabricated bandpass quad-channel diplexer-integrated PD.

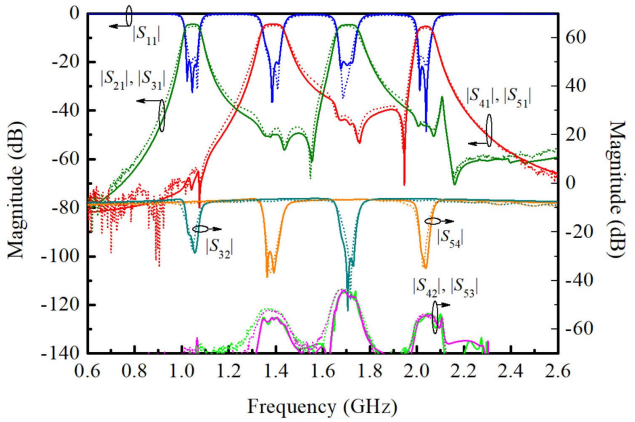

FIGURE 16. Simulated and measured frequency responses of proposed bandpass quad-channel diplexer-integrated PD. (simulation: solid curves; measurement: dotted curves).

in Table 4. The circuit was 0.81 $\lambda_g \times 0.35\ \lambda_g$ (152 mm × 66.3 mm), where λ_g is the guided wavelength at 1.05 GHz.

Figs. 16, 17, and 18 present the simulated and measured results for the proposed bandpass quad-channel diplexer-integrated PD. The proposed five-port circuit provides a third-order filtering function with equal-power division for each channel passband. The measured in-band return loss ($-20 \log |S_{11}|$) was larger than 17 dB. Including the 3-dB equal-power division loss, the insertion losses at channel passbands *I* and *III* ($-20 \log |S_{21}|$) were approximately $(3 + 2.3)$ and $(3 + 2)$ dB, respectively, and those at channel passbands *II* and *IV* ($-20 \log |S_{41}|$) were approximately $(3 + 2.1)$ and $(3 + 2.9)$ dB, respectively. The measured in-band group delay for the first, second, third, and fourth channel passbands are 9.24–10.1 ns, 6.91–7.87 ns, 7.07–8.7 ns, and 8.72–10.25 ns, respectively. Amplitude imbalances $|S_{21}| - |S_{31}|$ and $|S_{41}| - |S_{51}|$ were <0.1 dB, and phase imbalances $\angle S_{21} - \angle S_{31}$ and $\angle S_{41} - \angle S_{51}$ were <2°. The isolations between the output ports ($-20 \log |S_{32}|$ and $-20 \log |S_{54}|$) were >25 dB over the entirety of channel passbands *I*, *II*, *III*, and *IV*. The port isolations between different channels ($-20 \log |S_{42}|$ and $-20 \log |S_{53}|$) were all >40 dB. The high consistency between the measured and simulated performance serves as experimental validation of the proposed design.

IV. COMPARISON AND DISCUSSION

Table 5 presents a comparison of the proposed bandpass triplexer-integrated PD (case 1) and the proposed bandpass

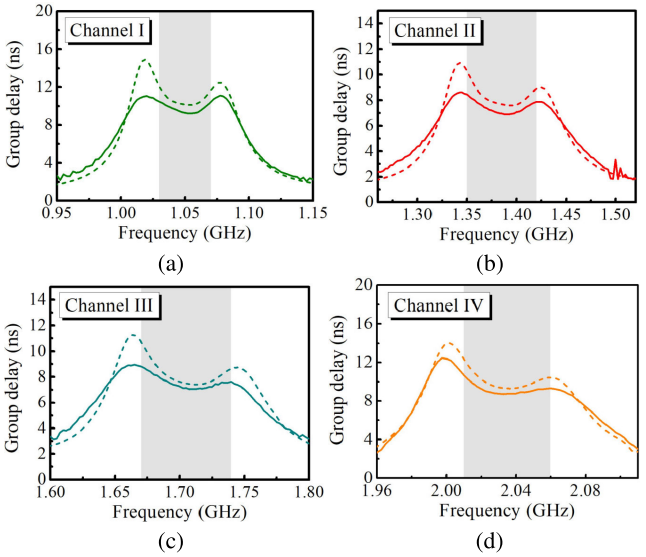

FIGURE 17. Simulated (dashed lines) and measured (solid lines) group delay of proposed bandpass quad-channel diplexer-integrated PD for (a) channel I, (b) channel II, (c) channel III, and (d) channel IV.

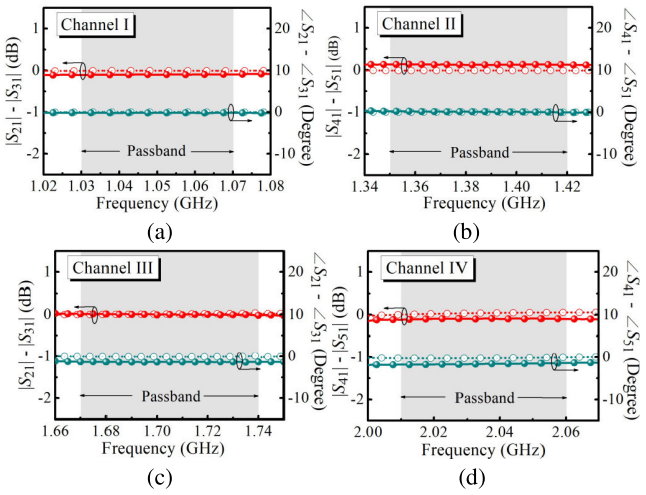

FIGURE 18. Magnitude and phase imbalances for (a) channel I, (b) channel II, (c) channel III, and (d) channel IV. (simulation: solid curves; measurement: dotted curves).

quad-channel diplexer-integrated PD (case 2) with similar devices reported in other studies. The advantages of the proposed bandpass multiplexer-integrated PD are as follows:

1) **Multifunctionality and high integration:**
The proposed bandpass multiplexer-integrated PD offers frequency division, frequency selection, and power splitting without a considerable increase in size. It can improve system integration and thereby reduce the system size and cost. Thus, the multifunctional PD can be used in numerous applications.
2) **More operating channels:**
The device in this study has more operating channels than do those in [37]–[42], which increases its applicability to multiband and multiservice wireless communication systems.

TABLE 5. Comparison with similar circuits.

	Ch	CF (GHz)	FBW (%)	FO	IL (dB)	Iso (dB)	Size (λ_g^2)
Case 1	3	1.31, 1.845, 2.2	6.0, 4.8, 2.2	3	4.0, 3.9, 5.9	> 25	0.29
Case 2	4	1.05, 1.4, 1.72, 2.05	5.7, 6.4, 5.2, 3.4	3	5.3, 5, 5.1, 5.9	> 25	0.28
[37]	2	1.77, 2.4	Not reported	2	3.7, 4	> 20	> 0.3
[38]	2	2.5, 3	Not reported	2	4.6, 4.9	> 21	0.2
[39]	2	1, 1.15	3.5, 3.6	2	3.7, 3.8	> 28	0.26
[40]	2	1.8, 2.4	6.3, 6.3	2	4.8, 4.8	> 20	> 0.8
[41]	3	1.64, 2.35, 3.03	18, 11, 8.2	2	3.2, 3.5, 3.5	> 13	> 0.3
[42]	2	1.525, 2.125	3.7, 3	2	4.2, 4.6	> 23	0.098

Ch, channels; CF, center frequency; FBW, fractional bandwidth; FO, filter order; IL, insertion loss; Iso, isolation

3) **Strong performance and compactness:**
All devices in [37]–[42] had a second-order filtering response. In this study, both the proposed triplexer-integrated PD and quad-channel diplexer-integrated PD were designed to have a third-order filtering response with favorable port-to-port isolation to increase responsiveness and selectivity. Because the dual-mode stub-loaded resonators (that serve different channel passbands) were used in the bandpass multiplexer-integrated PD, the number of resonators was low, enabling a considerable size reduction.

4) **Simple design and layout:**
The proposed design procedure is simple; the traditional coupled-resonator design method described in [44] can be directly applied. In addition, the structures do not require any via holes or slotted ground planes; thus, the device is easy to fabricate.

V. CONCLUSION

This study presented a novel methodology for designing bandpass multiplexer-integrated PDs. A bandpass triplexer-integrated PD and a bandpass quad-channel diplexer-integrated PD were designed, fabricated, and measured to verify the methodology. The experimental results were consistent with the EM simulation results. The proposed multifunctional bandpass multiplexer-integrated PD is compact, highly integrated, high performing, easy to design, and easy to fabricate.

REFERENCES

[1] P. Cheong, K. Lai, and K. Tam, "Compact Wilkinson power divider with simultaneous bandpass response and harmonic suppression," in *IEEE MTT-S Int. Microw. Symp. Dig.*, Anaheim, CA, USA, May 2010, pp. 1588–1591.
[2] J.-Y. Shao, S.-C. Huang, and Y.-H. Pang, "Wilkinson power divider incorporating quasi-elliptic filters for improved out-of-band rejection," *Electron. Lett.*, vol. 47, no. 23, pp. 1288–1289, Nov. 2011.
[3] X. Y. Zhang, K.-X. Wang, and B.-J. Hu, "Compact filtering power divider with enhanced second-harmonic suppression," *IEEE Microw. Wireless Compon. Lett.*, vol. 23, no. 9, pp. 483–485, Sep. 2013.
[4] C.-F. Chen, T.-Y. Huang, T.-M. Shen, and R.-B. Wu, "Design of miniaturized filtering power dividers for system-in-a-package," *IEEE Compon., Packag., Manuf. Technol.*, vol. 3, no. 10, pp. 1663–1672, Oct. 2013.
[5] C.-F. Chen and C.-Y. Lin, "Compact microstrip filtering power dividers with good in-band isolation performance," *IEEE Microw. Wireless Compon. Lett.*, vol. 24, no. 1, pp. 17–19, Jan. 2014.
[6] W.-M. Chau, K.-W. Hsu, and W.-H. Tu, "Filter-based Wilkinson power divider," *IEEE Microw. Wireless Compon. Lett.*, vol. 24, no. 4, pp. 239–241, Jul. 2018.
[7] X. Wang, J. Wang, and G. Zhang, "Design of wideband filtering power divider with high selectivity and good isolation," *Electron. Lett.*, vol. 52, no. 16, pp. 1389–1391, Aug. 2016.
[8] G. Zhang, J. Wang, L. Zhu, and W. Wu, "Dual-mode filtering power divider with high passband selectivity and wide upper stopband," *IEEE Microw. Wireless Compon. Lett.*, vol. 27, no. 7, pp. 642–644, Jul. 2017.
[9] X. Wang, J. Wang, G. Zhang, J. Hong, and W. Wu, "Design of out-of-phase filtering power divider based on slotline and microstrip resonator," *IEEE Trans. Compon., Packag., Manuf. Technol.*, vol. 9, no. 6, pp. 1094–1102, Jun. 2019.
[10] G. Zhang, X. D. Wang, J.-S. Hong, and J. Q. Yang, "A high-performance dual-mode filtering power divider with simple layout," *IEEE Microw. Wireless Compon. Lett.*, vol. 28, no. 2, pp. 120–122, Feb. 2018.
[11] C. Zhu, J. Xu, and W. Wu, "Microstrip four-way reconfigurable single/dual/wideband filtering power divider with tunable frequency, bandwidth, and PDR," *IEEE Trans. Ind. Electron.*, vol. 65, no. 11, pp. 8840–8850, Nov. 2018.
[12] G. Zhang, Z. Qian, J. Yang, and J.-S. Hong, "Wideband four-way filtering power divider with sharp selectivity and high isolation using coshared multi-mode resonators," *IEEE Microw. Wireless Compon. Lett.*, vol. 29, no. 10, pp. 641–644, Oct. 2019.
[13] G. Zhang, X. Zhang, Z. Qian, and J. Yang, "Analysis and design of compact four-way single- and dual-band filtering power dividers on a new adjustable multi-mode topology," *IET Microw., Antennas Propag.*, vol. 14, no. 5, pp. 381–389, Feb. 2020.
[14] G. Zhang, Z. Qian, X. Zhang, and J. Yang, "A general and effective design method of multi-way filtering power dividers on a new multi-port topology for industrial application," *IEEE Trans. Ind. Electron.*, vol. 68, no. 6, pp. 5436–5447, Jun. 2021.
[15] C. Zhu, J. Xu, W. Kang, and W. Wu, "Microstrip multifunctional reconfigurable wideband filtering power divider with tunable center frequency, bandwidth, and power division," *IEEE Trans. Microw. Theory Techn.*, vol. 66, no. 6, pp. 2800–2813, Jun. 2018.
[16] C. Cai, J. Wang, Y. Deng, and J.-L. Li, "Design of compact dual-mode dual-band filtering power divider with high selectivity," *Electron. Lett.*, vol. 51, no. 22, pp. 1795–1796, Oct. 2015.
[17] G. Zhang, J. Wang, L. Zhu, and W. Wu, "Dual-band filtering power divider with high selectivity and good isolation," *IEEE Microw. Wireless Compon. Lett.*, vol. 26, no. 10, pp. 774–776, Oct. 2016.
[18] Q. Li, Y. Zhang, and C.-T. M. Wu, "High-selectivity and miniaturized filtering Wilkinson power dividers integrated with multimode resonators," *IEEE Trans. Compon., Packag., Manuf. Technol.*, vol. 7, no. 12, pp. 1990–1997, Dec. 2017.
[19] G. Zhang, X. Wang, and J. Yang, "Dual-band microstrip filtering power divider based on one single multimode resonator," *IEEE Microw. Wireless Compon. Lett.*, vol. 28, no. 10, pp. 891–893, Oct. 2018.
[20] H. Lv, Q. Huang, and X. Shi, "Dual-band power divider using stub-loaded quad-mode resonator," in *Proc. Int. Conf. Microw. Millim. Wave Technol. (ICMMT)*, Guangzhou, China, May 2019, pp. 1–3.
[21] C.-F. Chen, C.-Y. Lin, B.-H. Tseng, and S.-F. Chang, "Compact microstrip electronically tunable power divider with Chebyshev bandpass response," in *Proc. Asia–Pacific Microw. Conf.*, Nov. 2014, pp. 1291–1293.
[22] P.-L. Chi and T. Yang, "A 1.3–2.08 GHz filtering power divider with bandwidth control and high in-band isolation," *IEEE Microw. Wireless Compon. Lett.*, vol. 26, no. 6, pp. 407–409, Jun. 2016.
[23] D. Psychogiou, R. Gómez-García, A. C. Guyette, and D. Peroulis, "Reconfigurable single/multi-band filtering power divider based on quasi-bandpass sections," *IEEE Microw. Wireless Compon. Lett.*, vol. 26, no. 9, pp. 684–686, Sep. 2016.
[24] R. Gómez-García, D. Psychogiou, and D. Peroulis, "Fully-tunable filtering power dividers exploiting dynamic transmission-zero allocation," *IET Microw., Antenna Propag.*, vol. 11, no. 3, pp. 378–385, Feb. 2017.
[25] G. Zhang, S. Liu, W. Chen, Z. Zhang, and J. Yang, "Design method for compact multifunctional reconfigurable filtering power divider on a new tunable three-port multi-mode topology," *IEEE Trans. Circuits Syst. I, Reg. Papers*, vol. 67, no. 12, pp. 4580–4592, Dec. 2020.
[26] B. Zhang and Y. Liu, "Wideband filtering power divider with high selectivity," *Electron. Lett*, vol. 51, no. 23, pp. 1950–1952, Nov. 2015.

[27] Y. Wu, Z. Zhuang, Y. Liu, L. Deng, and Z. Ghassemlooy, "Wideband filtering power divider with ultra-wideband harmonic suppression and isolation," *IEEE Access*, vol. 4, pp. 6876–6882, 2016.
[28] M.-T. Chen and C.-W. Tang, "Design of the filtering power divider with a wide passband and stopband," *IEEE Microw. Wireless Compon. Lett.*, vol. 28, no. 7, pp. 570–572, Jul. 2018.
[29] Y. C. Li, Q. Xue, and X. Y. Zhang, "Single- and dual-band power dividers integrated with bandpass filters," *IEEE Trans. Microw. Theory Techn.*, vol. 61, no. 1, pp. 69–76, Jan. 2013.
[30] Q. Li, Y. Zhang, and Y. Fan, "Dual-band in-phase filtering power dividers integrated with stub-loaded resonators," *IET Microw., Antennas Propag.*, vol. 9, no. 7, pp. 695–699, May 2015.
[31] C. Shao, Y. Li, and J.-X. Chen, "Compact dual-band microstrip filtering power divider using T-junction structure and quarter-wavelength SIR," *Electron. Lett.*, vol. 53, no. 6, pp. 434–436, Jan. 2017.
[32] Y. L. Wu, Z. Zhuang, G. Y. Yan, Y. A. Liu, and Z. Ghassemlooy, "Generalized dual-band unequal filtering power divider with independently controllable bandwidth," *IEEE Trans. Microw. Theory Techn.*, vol. 65, no. 10, pp. 3838–3848, Oct. 2017.
[33] X. Wang, J. Wang, G. Zhang, J.-S. Hong, and W. Wu, "Dual-wideband filtering power divider with good isolation and high selectivity," *IEEE Microw. Wireless Compon. Lett.*, vol. 27, no. 12, pp. 1071–1073, Dec. 2017.
[34] P. Wen, Z. Ma, H. Liu, S. Zhu, B. Ren, Y. Song, X. Wang, and M. Ohira, "Dual-band filtering power divider using dual-resonance resonators with ultrawide stopband and good isolation," *IEEE Microw. Wireless Compon. Lett.*, vol. 29, no. 2, pp. 101–103, Feb. 2019.
[35] P.-L. Chi, Y.-M. Chen, and T. Yang, "Single-layer dual-band balanced substrate-integrated waveguide filtering power divider for 5G millimeter-wave applications," *IEEE Microw. Wireless Compon. Lett.*, vol. 30, no. 6, pp. 585–588, Jun. 2020.
[36] J. Zheng, G. Zhang, X. Zhou, C. Xie, Y. Zhang, X. Wang, Y. Liu, W. Tang, and J. Yang, "Dual-band filtering power divider based on CSRRs loaded SIW cavity," *IEEE Trans. Circuits Syst. II, Exp. Briefs*, vol. 69, no. 2, pp. 394–398, Feb. 2022.
[37] P.-H. Deng, W. Lo, B.-L. Chen, and C.-H. Lin, "Designs of diplexing power dividers," *IEEE Access*, vol. 6, pp. 3872–3881, 2018.
[38] G. Zhang, Z. Qian, and J. Yang, "Design of a compact microstrip power-divider diplexer with simple layout," *Electron. Lett.*, vol. 54, no. 16, pp. 1007–1009, Apr. 2014.
[39] C.-F. Chen, K.-W. Zhou, R.-Y. Chen, Z.-C. Wang, and Y.-H. He, "Design of a microstrip diplexer-integrated filtering power divider," *IEEE Access*, vol. 7, pp. 106514–106520, 2019.
[40] C.-H. Lin, P.-H. Deng, and W.-T. Chen, "Design of a microstrip diplexing filtering power divider," in *Proc. IEEE Asia–Pacific Microw. Conf. (APMC)*, Singapore, Dec. 2019, pp. 944–946.
[41] L. Tang, X. Zhang, F. Jiao, S. Liu, G. Zhang, and J. Yang, "Design of a compact microstrip triplexer-power divider with E-shaped resonator," in *Proc. Int. Conf. Microw. Millim. Wave Technol. (ICMMT)*, Guangzhou, China, May 2019, pp. 1–3.
[42] C.-F. Chen, K.-W. Zhou, R.-Y. Chen, H.-Y. Tseng, Y.-H. He, W.-J. Li, and J.-H. Weng, "Design of microstrip multifunction integrated diplexers with frequency division, frequency selection, and power division functions," *IEEE Access*, vol. 9, pp. 53232–53242, 2021.
[43] U. Rosenberg and S. Amari, "Novel coupling schemes for microwave resonator filters," *IEEE Trans. Microw. Theory Techn.*, vol. 50, no. 12, pp. 2896–2902, Dec. 2002.
[44] J. S. Hong and M. J. Lancaster, *Microstrip Filter for RF/Microwave Application*. New York, NY, USA: Wiley, 2001.

CHI-FENG CHEN (Member, IEEE) received the M.S. degree in electrophysics from the National Chiao Tung University, Hsinchu, Taiwan, in 2003, and the Ph.D. degree in communication engineering from the National Taiwan University, Taipei, Taiwan, in 2006.

From 2008 to 2010, he was a RF Engineer with Compal Communications Inc., Taipei, where he was involved in the research and development of global system for mobile communication (GSM) and code division multiple access (CDMA) mobile phones. In April 2010, he joined the Graduate Institute of Communication Engineering, National Taiwan University, as a Postdoctoral Research Fellow. Since 2012, he has been a Faculty Member with the Department of Electrical Engineering, Tunghai University (THU), Taichung, Taiwan, where he is currently a Professor. He is also the Chairperson of the Department of Electrical Engineering, THU. His research interests include the design of microwave circuits and associated RF modules for microwave and millimeter-wave applications.

Dr. Chen was a recipient of the THU Excellent Teaching Award, in 2020.

HSIN-YA TSENG was born in Tainan, Taiwan, in 1997. She is currently pursuing the M.S. degree with the Department of Electrical Engineering, Tunghai University, Taichung, Taiwan. Her current research interest includes the design of RF/microwave circuits.

YI-HUA HE was born in Taipei, Taiwan, in 1997. She is currently pursuing the M.S. degree with the Department of Electrical Engineering, Tunghai University, Taichung, Taiwan. Her current research interest includes the design of RF/microwave circuits.

WEN-JIE LE was born in Taoyuan, Taiwan, in 1998. She is currently pursuing the M.S. degree with the Department of Electrical Engineering, Tunghai University, Taichung, Taiwan. Her current research interest includes the design of RF/microwave circuits.